JACS Au
AN OPEN ACCESS JOURNAL OF THE AMERICAN CHEMICAL SOCIETY

Open Access
This article is licensed under CC-BY 4.0

pubs.acs.org/jacsau
Article

Simplified Preservation of Equivalent Pathways Spectroscopy

Evgeny Nimerovsky,* Abel Cherian Varkey, Myeongkyu Kim, Stefan Becker, and Loren B. Andreas*

Cite This: JACS Au 2023, 3, 2763−2771
Read Online

ACCESS | Metrics & More | Article Recommendations | Supporting Information

ABSTRACT: Inspired by the recently proposed transverse mixing optimal control pulses (TROP) approach for improving signal in multidimensional magic-angle spinning (MAS) NMR experiments, we present simplified preservation of equivalent pathways spectroscopy (SPEPS). It transfers both transverse components of magnetization that occur during indirect evolutions, theoretically enabling a $\sqrt{2}$ improvement in sensitivity for each such dimension. We compare SPEPS transfer with TROP and cross-polarization (CP) using membrane protein and fibril samples at MAS of 55 and 100 kHz. In three-dimensional (3D) (H)CANH spectra, SPEPS outperformed TROP and CP by factors of on average 1.16 and 1.69, respectively, for the membrane protein, but only a marginal improvement of 1.09 was observed for the fibril. These differences are discussed, making note of the longer transfer time used for CP, 14 ms, as compared with 2.9 and 3.6 ms for SPEPS and TROP, respectively. Using SPEPS for two transfers in the 3D (H)CANCO experiment resulted in an even larger benefit in signal intensity, with an average improvement of 1.82 as compared with CP. This results in multifold time savings, in particular considering the weaker peaks that are observed to benefit the most from SPEPS.

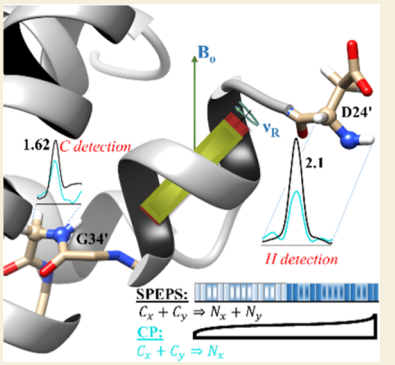

KEYWORDS: *magic-angle spinning, nuclear magnetic resonance spectroscopy, heteronuclear dipolar recoupling, SPEPS, preservation of equivalent pathways, FLAN conditions*

Downloaded via MPI MULTIDISCIPLINARY SCIENCES on January 10, 2024 at 10:33:36 (UTC).
See https://pubs.acs.org/sharingguidelines for options on how to legitimately share published articles.

INTRODUCTION

Heteronuclear recoupling elements are essential components of magic-angle spinning[1] (MAS) solid-state NMR experiments. These elements connect dipolar-coupled spin pairs,[2] allowing for the enhancement of low γ signals, and the dispersion of resonances in multidimensional spectra. Multidimensional experiments with dipolar recoupling elements at ultrafast MAS rates[3−7] with proton detection[8−12] are widely used for amino acid assignment and for structure determination and are applied in both materials and biological samples.[7,13−17]

The signal-to-noise ratio (SNR) of multidimensional experiments strongly depends on the efficiency of the recoupling elements. Traditionally, the cross-polarization (CP) element[18] is used to recouple heteronuclear dipolar interactions between spin pairs under Hartmann−Hahn conditions.[19] Initially, the element started as an experiment with constant power amplitude[20] and was subsequently modified to include modulation (most commonly a power ramp) to improve transfer efficiency and reduce the influence of experimental imperfections.[21−39] However, for low γ spin pairs like $^{13}C-^{15}N$, the experimental transfer efficiency of the conventional CP element is relatively low for nondeuterated biological samples.[17,40] It impacts the sensitivity of spectra used for amino acid assignments, especially when $^{13}C-^{15}N$ transfers are implemented twice in the same experiment.

Simultaneously transferring both components of the transverse magnetization between heteronuclear dipolar-coupled spin pairs is an elegant way to enhance SNR in multidimensional NMR experiments.[41] This sensitivity-enhancement method, dubbed "preservation of equivalent pathways" (PEP) was proposed by Cavanagh and Rance in 1990[42] for liquid-state NMR. The two components are acquired together, but with alternation of the sign of one component every other scan such that the real and imaginary components can be deconvoluted during data processing—a procedure known as echo/anti-echo mode acquisition.[43] The measured signal contains contributions from both transverse components, rotated by an isotropic chemical shift interaction during the indirect dimension. In ideal cases, this provides a $\sqrt{2}$ improvement in SNR,[42,44,45] compared to similar experiments where the amplitude of only one transverse component was recorded.

In liquid-state NMR experiments, the J-coupling interaction[46] is usually used to transfer both transverse components between spin pairs.[42,44] For solid-state NMR, dipolar couplings are recoupled in the conventional CP element,[19,38] which transfers only one of the components between dipolar-coupled spin pairs. Therefore, until recently, the PEP scheme had been mainly incorporated into solid-state experiments with recoupling of

Received: June 15, 2023
Revised: September 27, 2023
Accepted: September 27, 2023
Published: October 11, 2023

ACS Publications
© 2023 The Authors. Published by American Chemical Society

https://doi.org/10.1021/jacsau.3c00312
JACS Au 2023, 3, 2763−2771

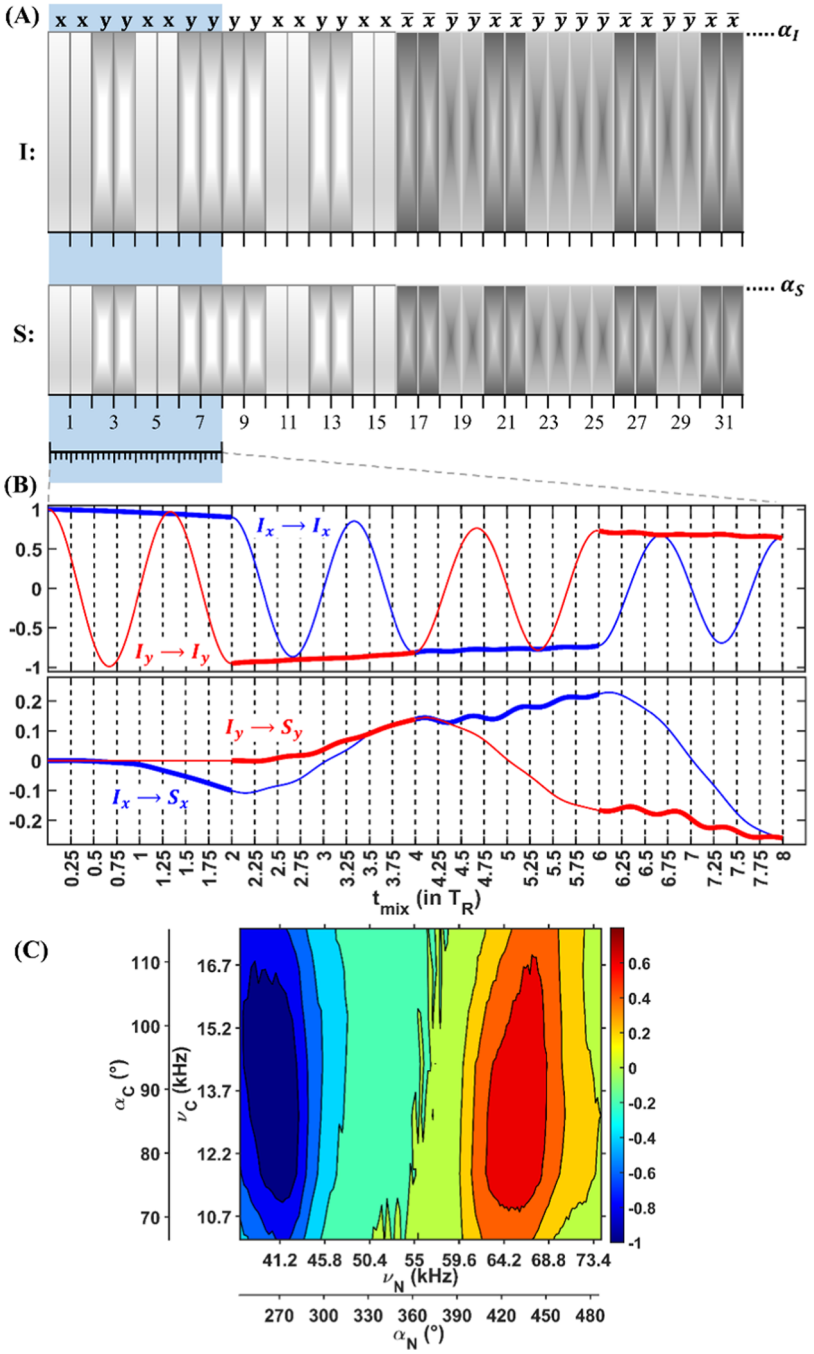

Figure 1. ^{13}CA → ^{15}N SPEPS. (A) Each repeated SPEPS element consists of 32 pulses, with each pulse having the length of one rotor period (T_R) and flip angles: α_I ($\alpha_I = \nu_I T_R$) and α_S ($\alpha_S = \nu_S T_R$) on I and S channels, respectively ($T_R = 1/\nu_R$, ν_R is MAS in kHz). (B) Simulated evolution of I_x, I_y, S_x, and S_y operators during the first eight rotor periods. (C) Experimental signal intensity of the ^{13}C−^{15}N transfer (at t_{mix} = 2.91 ms) as a function of the applied rf-field strengths (flip angle values). The data were acquired on a 600 MHz spectrometer with 55 kHz MAS using the S31N M2 sample. Further details of simulations and experiments are presented in the Experimental Methods Section and in the SI.

homonuclear correlations,[47−49] γ-prepared elements,[50−52] or for static/oriented samples.[53−56]

In 2022, Blahut et al.[41] introduced the transverse mixing optimal control pulses (TROP), which simultaneously transferred both transverse components via dipolar couplings. They showed that for deuterated samples, the gain in SNR could be more than $\sqrt{2}$ for each indirect dimension.

Inspired by their work, we have developed simplified preservation of equivalent pathways spectroscopy (SPEPS) for the simultaneous transfer of both transverse components. We demonstrate it in nondeuterated samples. The element has a simple structure, a straightforward optimization procedure, and is robust with respect to radiofrequency field (rf-field) mismatches. It is particularly efficient for resonances that appear to be negatively affected by dynamics or high-proton-density environments in the CP spectra.

RESULTS AND DISCUSSION

The basic SPEPS element is depicted in Figure 1A. It contains 32 rotor-synchronized pulses, each with a length of one rotor

https://doi.org/10.1021/jacsau.3c00312
JACS Au 2023, 3, 2763−2771

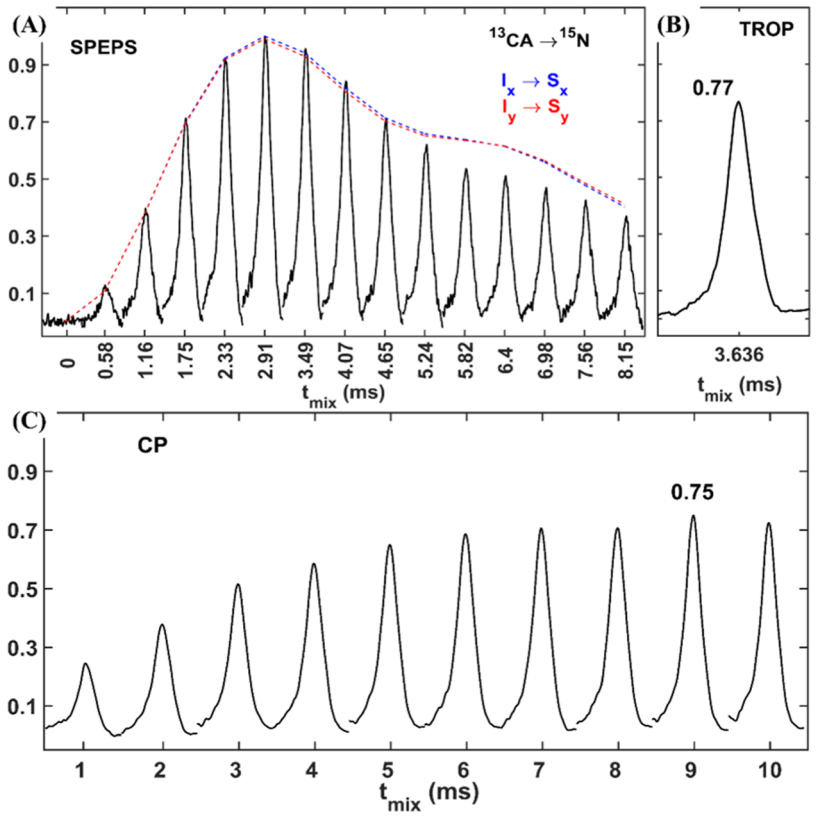

Figure 2. $^{13}CA \rightarrow {}^{15}N$ buildup curves, normalized to the SPEPS maximum intensity. (A) Simulated SPEPS ($I_x \rightarrow S_x$ blue and $I_y \rightarrow S_y$ red) and experimental (average $I_x \rightarrow S_x$ and $I_y \rightarrow S_y$ black spectra) transfer efficiency plotted against mixing time. In the simulations, a three-spin system (I_2S) was used with heteronuclear and homonuclear dipolar coupling values of 1.1 and 2.5 kHz, respectively. Pulses of 284° (43.4 kHz) and 79° (12.1 kHz) were applied on the I and S channels, respectively. (B) Experimental TROP spectrum at a fixed 3.636 ms mixing time for 55 kHz MAS. (C) Experimental CP transfer efficiency plotted against mixing time. In all figures, all experimental spectra have been normalized using the maximal intensity obtained from the SPEPS experiments. The data were acquired on a 600 MHz spectrometer with 55 kHz MAS and the S31N M2 sample. In the experiments, the global SPEPS phase cycling was shifted by 90° from scan to scan to balance the *x*- and *y*-component transfer efficiency. Further details of simulations and experiments are presented in the Experimental Methods Section and in the SI.

period. The phase cycling of the pulses on both channels is identical and equals: $x,x,y,y,x,x,y,y,y,y,x,x,y,y,x,x,\bar{x},\bar{x},\bar{y},\bar{y},\bar{x},\bar{x},\bar{y},\bar{y},\bar{y},\bar{y},\bar{x},\bar{x},\bar{y},\bar{y},\bar{x},\bar{x}$ (XY-16 based phase cycling[57]). The basic element can be extended in length by repetition, allowing facile application over a range of spinning frequencies. The flip angle values of each pulse on the I and S channels are α_I ($\alpha_I = \nu_I T_R$) and α_S ($\alpha_S = \nu_S T_R$), respectively ($T_R = 1/\nu_R$, ν_R is MAS in kHz). The optimal flip angles of the pulses are the flip angles that fulfill the FLAN conditions[58] (briefly explained in the Supporting Information (SI)) and Hartmann−Hahn conditions[19] simultaneously (Figure S1 in the SI). For example, possible optimal rf-field strengths (in kHz) for double-quantum (DQ) and zero-quantum (ZQ) transfers are (0.25, 0.75 ν_R) and (0.25, 1.25 ν_R), respectively. Herein, we focus primarily on the DQ condition, which has a low rf-field requirement for both rf channels.

Figure 1B shows simulations that explain the mechanism of simultaneous transfer of both transverse components, showing evolutions of transverse (I_x, I_y) and (S_x, S_y) operators during the first eight rotor periods. When the initial operator, I_j ($j = x$ or y), has the same phase as the applied rf-field pulses, the operator becomes locked and the transfer from I_j to S_j occurs (indicated by thick lines). When the initial operator and the applied pulse phase differ by 90°, the I_j operator is inverted after two rotor periods have elapsed (indicated by thin lines). This construction enables the simultaneous transfer of $I_x \rightarrow S_x$ and $I_y \rightarrow S_y$ operators within the SPEPS pulse. It also results in a slower transfer of magnetization. However, the experimental optimum transfer time for ramped CP is also long such that the optimal transfer time for SPEPS ends up shorter than that for ramped CP (vide infra).

A successful pulse sequence must be robust against rf-field mismatches or inhomogeneity and should remain effective for a range of spin systems. Fortunately, the requirement for complete inversion of the nontransferred spins is relaxed when the SPEPS element is implemented with the full, extended, phase cycling scheme, as shown in Figures S2 and S3 in the SI. Figure S4 shows that there is a small dependence of the SPEPS element on the number of proximate proton spins and on the rf-field inhomogeneity.

Experimental data confirm the performance of SPEPS. From the experimental SPEPS profile (Figure 1C), we observe two regions of optimal RF-field strengths on the I and S channels for DQ (negative) and ZQ (positive) transitions: 0.24, 0.75 and 0.24, 1.21 ν_R. Our focus was on SPECIFIC CP[22,59] such that we did not consider higher rf-field on the ^{13}C channel. The DQ condition also appears to be more efficient than the ZQ condition (Figure S5 in the SI).

Figure 2 shows SPEPS (Figure 2A) and CP (Figure 2C) signal intensity as a function of mixing time as well as the TROP spectrum (Figure 2B). TROP is a transfer element designed with

https://doi.org/10.1021/jacsau.3c00312
JACS Au 2023, 3, 2763−2771

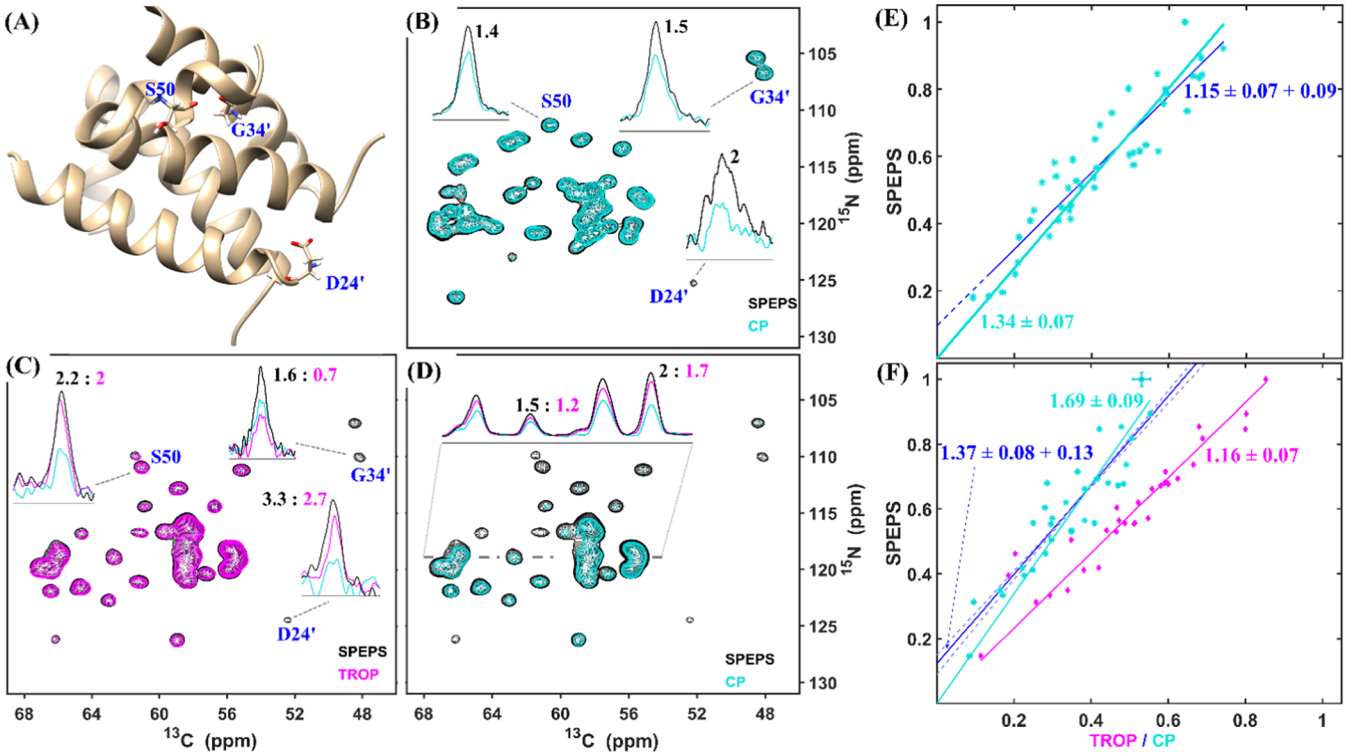

Figure 3. Comparison of 3D (H)CANH spectra recorded with SPEPS, TROP, and CP for the M2 protein from Influenza A. (A) Structure of influenza A M2 from PDB 2N70.[72] (B, E), 950 MHz data at 100 kHz MAS recorded for WT M2. (C, D, F), 850 MHz data at 55 kHz MAS recorded for S31N M2. (B–D) ^{13}C–^{15}N projections from 3D spectra obtained with SPEPS (black), TROP (magenta), and CP (cyan) elements for ^{13}C–^{15}N transfers. (E, F) Comparison of the peak intensities for selected residues: magenta – SPEPS (axis *y*) and TROP (axis *x*); cyan – SPEPS (axis *y*) and CP (axis *x*). The lines were obtained with linear least-squares fitting either with (cyan, magenta) or without (blue) fixing the intercept to zero. For (F), three pairs of residues were scaled down by a factor of 2 due to chemical shift degeneracy. Six Leucine residues were not included in the comparison due to signal overlap. The errors in the slopes were obtained by calculating the standard deviation values. The dashed lines represent the fitting lines with fixed slope values (from solid blue lines) ± errors. Further details of simulations and experiments are presented in the Experimental Methods Section and in the SI.

a fixed mixing time, while SPEPS and CP elements can be optimized with respect to time. The behaviors of the experimental and simulated SPEPS curves under the DQ conditions are in good agreement with each other (Figure 2A). In simulations (dashed lines, normalized to the maximum simulated intensity), a transfer efficiency of approximately 46% is observed as compared to the simulated 90° excitation. The same efficiency is simulated for each transverse component ($I_x \rightarrow S_x$ blue curves and $I_y \rightarrow S_y$ red curves). Experimentally, we estimated an efficiency of approximately 31% by comparison with a direct polarization (a 90° excitation; Figure S6 in the SI). For CP (Figure 2C), longer mixing times are required to reach maximal efficiency (9 ms) compared to that of SPEPS (2.91 ms). For this nondeuterated sample, SPEPS exhibits higher ^{13}C–^{15}N transfer efficiency compared to TROP and CP (SPEPS/TROP/CP – 1:0.77:0.75). In Figures S7–S8, we show the experimental optimization profiles for CP (Figure S7) and TROP (Figure S8), demonstrating that conditions were carefully adjusted to maximize the transfer in each case.

It is worth mentioning that in all experiments traditional ramped CP elements were used for ^{1}H–^{13}C and ^{1}H–^{15}N transfers. As investigated by different research groups,[34,60−68] the ramped CP elements result in a volume- and orientation-selective transfer due to rf-field inhomogeneity. The SPEPS element itself is also affected by rf-field inhomogeneity (Figure S4). We would therefore recommend to optimize all transfer elements of SPEPS-based sequences, rather than taking the optimization from the CP-only sequences. We did this for the data acquired at the 850 spectrometer, but not for the 600 MHz data, where the values from CP-only-based transfer were taken directly for the SPEPS-based sequences. The difference amounted to 5 to 10% at the 850 MHz instrument.

Figure S9 shows one-dimensional (1D) comparisons of SPEPS, TROP, and CP showing improved performance for SPEPS for ^{13}C–^{15}N transfer compared to CP and TROP at an 850 MHz spectrometer using 55 kHz MAS (Figure S9A) and a similar transfer efficiency compared to CP at a 950 MHz spectrometer using 100 kHz MAS (Figure S9B). By contrast, CP remained the most efficient for ^{15}N–^{1}H transfer (Figure S10). Nominally, only a single transverse component is transferred in all of these 1D experiments.

At 55 kHz and 850 MHz (Figure S9A), SPEPS exhibits higher ^{13}C–^{15}N transfer efficiency compared to TROP and CP (SPEPS/TROP/CP – 1:0.81:0.85). Similar 1D signals were seen for SPEPS and CP at 100 kHz (Figure S9B), indicating that SPEPS should outperform CP in multidimensional spectra. The TROP element was not investigated at 100 kHz MAS due to the limitations of the rf-field powers of the probe, and since a suitable TROP pulse has not been reported for 100 kHz MAS.

In Figure S11, we present comparisons of 2D SPEPS, TROP, and CP spectra with nitrogen and carbon detection. Here, we expect a $\sqrt{2}$ gain in SNR for SPEPS and TROP elements as compared with the 1D signal of Figure S9 since SPEPS and TROP transfer both transverse components of magnetization. For ^{13}C → ^{15}N transfers (Figure S11A), SPEPS is notably more efficient than the TROP element for residues with a high-

https://doi.org/10.1021/jacsau.3c00312
JACS Au 2023, 3, 2763−2771

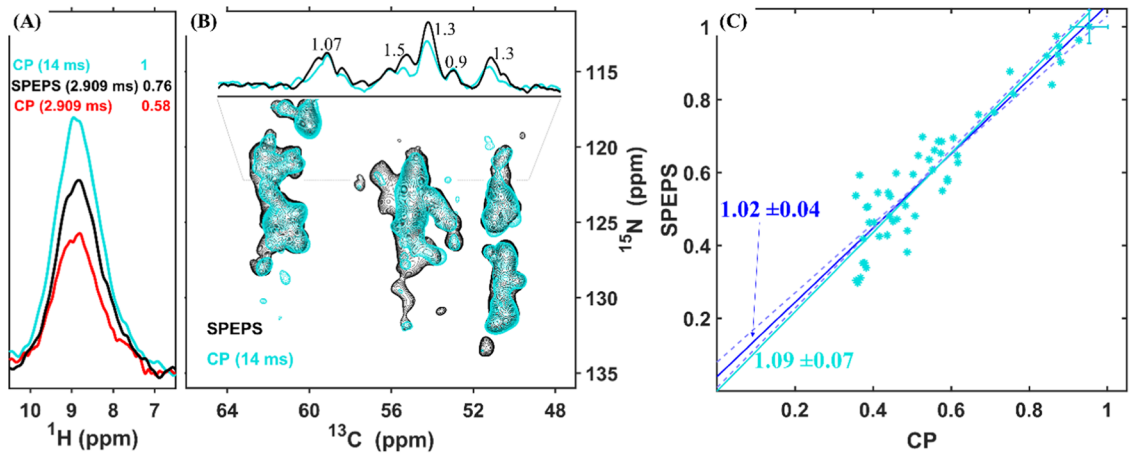

Figure 4. Comparison of 3D (H)CANH spectra recorded with SPEPS and CP for the α-Synuclein fibril. (A) 1D (HCAN)H spectra with CP (2.909 ms, red and 14 ms, cyan) and SPEPS (2.909, black) elements. (B) ^{13}C−^{15}N projections from 3D spectra obtained with SPEPS (black) and CP (14 ms, cyan) elements for ^{13}C−^{15}N transfers. (C) Comparison of peak intensities for all peaks detected above the noise threshold of the CP experiment: SPEPS (y-axis) and CP (x-axis). The lines were obtained with linear least-squares fitting either with (cyan) or without (blue) fixing the intercept to zero. The data were acquired using an 850 MHz spectrometer with 55 kHz MAS. Further details of simulations and experiments are presented in the Experimental Methods Section and in SI.

proton-density environment[69] (e.g., glycine and proline residues). For ^{15}N → ^{13}C transfers (Figure S11C), SPEPS demonstrates much higher transfer efficiency compared to TROP and CP. This is unsurprising for the TROP element since it was specifically developed for ^{13}C → ^{15}N transfer.[69]

The ^{13}C−^{15}N SPEPS element can be incorporated into the proton-detected three-dimensional (3D) (H)CANH experiment, where ^{1}H−^{13}C and ^{15}N−^{1}H transfers are implemented with conventional CP elements. The data requires an echo/anti-echo-like manipulation in the time domain before Fourier transformation, as previously described.[70] A script for this purpose is provided in the SI as a .txt file and is combined with optional drift correction.[71]

Figure 3 displays the corresponding data recorded from the 3D (H)CANH experiments. The tetrameric arrangement of membrane protein influenza A M2 is shown in Figure 3A, with residues D24, G34, and S50 indicated. In Figure 3B−D, we present a comparison of ^{13}C−^{15}N projections from 3D (H)CANH spectra obtained using SPEPS (black), TROP (magenta), and CP (cyan) elements, acquired on a 950 MHz spectrometer, with 100 kHz MAS (B) and at 850 MHz, with 55 kHz MAS (C−D). Figure 3E,F compares all detected peak intensities from the SPEPS spectrum with the corresponding peaks from the CP (blue)- and TROP (magenta)-based spectra. Cyan and magenta lines in Figure 3E,F are linear fits with the y-intercept fixed to 0 and show the average improvement in peak intensity. The y-intercepts of the blue trend lines (linear fits of slope and intercept) indicate that the benefit of SPEPS is proportionally larger for weaker peaks. Note that the slope in this case does not indicate the improvement, and in fact, a slope of zero could be ideal, if all peaks in the SPEPS spectrum would be equally intense. The dashed lines define the range of possible y-intercept values, resulting after refitting the data with the slope plus, or minus, the error in the slope (dashed lines). Both dashed lines have positive y-intercepts, confirming the aforementioned conclusion. All errors are reported at 1 standard deviation.

The observation that SPEPS improves the signals of weaker peaks in the M2 spectra and the fact that SPEPS requires shorter transfer times than CP suggest that the benefit of SPEPS can be expected to be sample dependent. We therefore selected a fibrillar α-Synuclein sample and assessed the performance of SPEPS on an 850 MHz spectrometer (Figure 4) in comparison with CP. In Figure 4A, a comparison of 1D (HCAN)H spectra reveals a 1.3-fold higher signal using CP (14 ms, cyan) vs SPEPS (black). Notably, the CP optimum, at 14 ms, is longer than the optimum 9 ms for M2 (Figure 2), which is consistent with longer relaxation times and more ideal performance of CP. Consistent with the M2 data, at a shorter CP mixing time (red) that matches the optimum for SPEPS, a significantly lower signal is observed. Figure 4B presents a comparison of ^{13}C−^{15}N projections from a 3D (H)CANH experiment with SPEPS (black) and CP (14 ms mixing time, cyan) elements. Figure 4C compares all detected peak intensities from the CP spectrum to the corresponding peaks from the SPEPS-based spectrum. The additional $\sqrt{2}$ gain in SNR for the SPEPS element, obtained from acquiring the 3D (H)CANH experiment, results in the expected slight improvement over CP by a factor of 1.09 (Figure 4C).

It is worth noting that theoretical simulations that do not consider relaxation would predict a higher transfer efficiency for CP than for SPEPS. Adiabatic CP, with an efficiency up to 100%,[39,73,74] exceeds the simulated transfer efficiency of the SPEPS element, which suggests that for samples with very long relaxation times, SPEPS may not outperform CP. It appears that the fibrillar sample comes closer to this situation. Nevertheless, a slight improvement was observed with SPEPS, suggesting that it can be applied across different sample types (Table 1).

Table 1. Average SNR Improvement from the Three Samples[a]

sample	M2 WT	M2 S31N	αSYN
^{1}H Larmor frequency	950 MHz	850 MHz	850 MHz
MAS	100 kHz	55 kHz	55 kHz
SPEPS vs CP	1.34	1.69	1.09
SPEPS vs TROP		1.16	

[a]Summary of SNR improvement factors obtained from peak intensities of 3D (H)CANH spectra with SPEPS vs TROP or CP elements (Figures 3 and 4).

https://doi.org/10.1021/jacsau.3c00312
JACS Au 2023, 3, 2763−2771

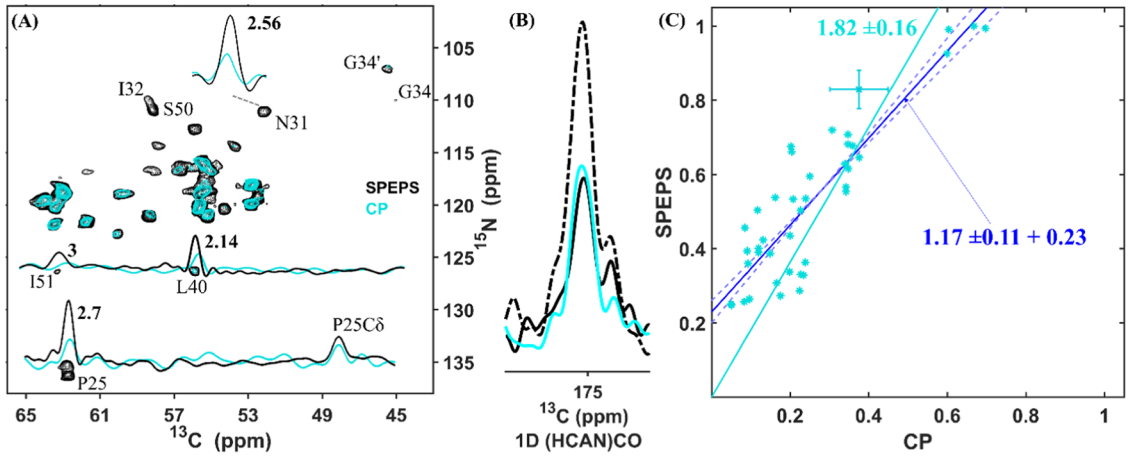

Figure 5. 3D (H)CANCO spectra of S31N M2 acquired with either SPEPS (black) or CP (cyan). (A) ^{13}C−^{15}N projections for spectra acquired with SPEPS (black) or CP (cyan) for ^{13}C−^{15}N transfers. (B) 1D (HCAN)CO spectra with SPEPS (solid black, only one component; dash-dot black, the sum of both components) and CP (cyan) elements. (C) Comparison of peak intensities for all peaks detected above the noise threshold: SPEPS (*y*-axis) and CP (*x*-axis). The lines were obtained with linear least-squares fitting either with (cyan) or without (blue) fixing the intercept to zero. The data were acquired using a 600 MHz spectrometer with 55 kHz MAS. The same ^{1}H−^{13}CA CP conditions were applied for both experiments. Further details of simulations and experiments are presented in the Experimental Methods Section and in the SI.

The 3D (H)CANCO spectrum is a more challenging case since it requires two magnetization transfers between carbon and nitrogen spins. This experiment can be crucial for site-specific assignment, as it links the three sequential backbone resonances.[75,76] However, the 3D (H)CANCO experiment is hindered by a characteristically low signal-to-noise ratio (SNR) and typically is recorded with large sample volumes or long experimental times.

The SPEPS element provides a practical solution to enhance the performance of the 3D (H)CANCO experiment. We observed an improvement in SNR by a factor of almost 2, as shown in Figure 5. From the 1D comparison, we observe a similar intensity for the SPEPS and CP elements (Figure 5B), when only one component is detected for the SPEPS (solid black). The sum of the signals from both components (dash-dot black) provides the expected 2-fold improvement in SNR. Figure 5A compares the CA-N projections from the 3D (H)CANCO experiments obtained with the SPEPS (black) and CP (cyan) elements. Figure 5C presents a comparison of the peak intensities using the SPEPS (*y*-axis) and CP (*x*-axis) elements. On average, SPEPS provides a 1.82-fold SNR improvement factor, slightly below the expectation of 2 based on the 1D comparison.

Also here, the *y*-intercept of 0.23 of the dark blue trend line in Figure 5C indicates that the benefit of SPEPS is proportionally larger for weaker peaks. This facilitates the interpretation of the spectrum since the weaker peaks become less likely to be obscured by overlapping signals. Furthermore, the required acquisition time is determined by the intensity of the weakest peak of interest. Since the required time scales with the square of the SNR, the observed improvement translates into a multiple-fold reduction in the required spectrometer time.

CONCLUSIONS

In summary, this work introduces the SPEPS transfer element, which improves SNR by transferring both components of magnetization that evolve in indirect dimensions. The SPEPS element has a simple structure and a facile optimized procedure and exhibits robust performance in the presence of rf-field inhomogeneity. We compared the transfer efficiency of SPEPS with the conventional CP element[38] and the recently proposed TROP element[41] and found a substantial improvement. A more impressive enhancement was seen for the 3D (H)CANCO experiment that contains two SPEPS transfers, where we observed an average SNR improvement factor of 1.82 compared to CP. The short transfer time of SPEPS is expected to facilitate measurements of peaks affected by short relaxation times during the transfer, such as may occur for residues with a high-proton-density environment or for nonideal membrane protein preparations. Indeed, a particular benefit was observed for the more challenging, low-intensity peaks, ultimately facilitating the NMR-based study of complex biomolecular systems with higher fidelity.

EXPERIMENTAL METHODS

Simulations

SPEPS simulations were performed using in-house MATLAB scripts to compute the numerical solution of the equation of motion.[77]

For simulations in Figure 1B, we used a two-spin system (representing CA and N spins) with 11 kHz dipolar coupling. For simulations in Figure 2A, a three-spin system (representing CO, CA, and N spins) was used with heteronuclear (CA-N) and homonuclear (CO-CA) dipolar coupling values of 1.1 and 2.5 kHz, respectively, and with the following values for [chemical shift offset; chemical shift anysotropy] in kHz: [−0.6;9] (N); [−1.7;8] (CA); and [15;17] (CO). Pulses of 284° (43.4 kHz) and 79° (12.1 kHz) were applied on the *N* and *C* channels, respectively, slightly away from the expectation of 270 and 90° such that each pulse produces a net 180° rotation over two rotor periods.

Sample Preparation

Influenza A M2 Samples. Influenza A wild-type M2 and S31N M2 proteins (residues 18−60) were prepared according to the protocols in the references.[78,79] The samples were packed into either Bruker 1.3 or 0.7 mm rotors via centrifugation.

***α*-Synuclein Sample.** *α*-Synuclein was recombinantly produced in *Escherichia coli* strain BL21(DE3) as previously described.[80] ^{13}C,^{15}N-labeled samples were expressed in a minimal medium supplemented with $^{15}NH_4Cl$ and $^{13}C_6$-D-glucose (Cambridge Isotope Laboratories and Sigma-Aldrich). The protein was finally dialyzed against buffer (50 mM HEPES, 100 mM NaCl, pH 7.4) to obtain a 0.3 mM solution, and the resulting solution was stored at −80 °C until use.

https://doi.org/10.1021/jacsau.3c00312
JACS Au 2023, 3, 2763−2771

Vesicles were prepared from lipid films. A chloroform mixture of 1-palmitoyl-2-oleoyl-glycero-3-phosphocholine (POPC), 1-palmitoyl-2-oleoyl-*sn*-glycero-3-phosphate (POPA) was placed under a N_2-stream to form lipid films, and the film was lyophilized overnight. Buffer (50 mM HEPES, 100 mM NaCl, pH 7.4) was added, and SUVs were obtained by repeated sonication to produce a solution of 1.5 mM POPC and 1.5 mM POPA.

Monomeric α-synuclein (in buffer containing 50 mM Hepes, 100 mM NaCl, and pH 7.4) was centrifuged for 1 h at 55,000 rpm using a TLA-100.3 rotor in an Optima MAX-XP tabletop ultracentrifuge (both Beckman Coulter) at 4 °C. The supernatant was added to a solution of phospholipid small unilamellar vesicles (SUVs) and NaN_3 (0.02 wt %) to obtain a final protein concentration of 70 μM and a molar lipid-to-protein ratio of 10 in buffer (50 mM HEPES, 100 mM NaCl, pH 7.4) and continuously shaken with 1% (molar ratio) preformed fibril seeds at 180 rpm in a Multitron incubator (Infors HT, Bottmingen, CH). The seeds were obtained by sonicating preformed a-Syn fibrils that were prepared previously.[81] After 96 h, the fibrils were harvested by centrifuging at 152,460*g* (TLA-100.3 rotor in an OptimaTM MAX-TL) for 1 h at 4 °C. The supernatant was removed, and the resulting pellet was washed with fresh buffer and centrifuged again at 212,940*g* for 10 min at 18 °C. Excess moisture was removed, and the pellet was immediately packed into a 1.3 mm rotor.

Solid-State NMR Spectroscopy

Optimizing SPEPS Experiments. ^{13}C and ^{15}N 90° hard pulses were precisely calibrated (crucial for such experiments, where the pair of 90° pulses preceding the SPEPS transfer inverts the transverse component in alternating increments). The initial rf-field power values of the SPEPS element were set according to hard pulse calibrations and optimized empirically around these values. For ^{13}C and ^{15}N channels, the optimal rf-field values correspond to approximately 0.25 and 0.75 ν_R, respectively. The carrier frequencies of ^{13}CA and ^{15}N were set to 53.7 and 116 ppm, respectively.

600 MHz. 1D (HCAN)H (Figures 1C and 2) and 3D (H)CANCO (Figure 5) experiments were acquired on a Bruker Avance III HD spectrometer operating at 14.1 T (600 MHz ^1H frequency) using a DVT600W2 BL1.3 mm HXY probe. The experiments were performed at 55 kHz MAS, and the temperature of the nitrogen cooling gas was set to 245 K with 1000 to 1300 L/h.

850 MHz. 3D (H)CANH experiments (Figures 3C–D and 4) were acquired on an Avance III spectrometer operating at 19.97 T (850 MHz ^1H field strength), equipped with a 1.3 mm HCN MAS probe at 55 kHz MAS. The temperature of the nitrogen cooling gas was set to 245 K.

950 MHz. 3D (H)CANH experiments (Figure 3B) were acquired on a Bruker Avance III HD spectrometer operating at 22.3 T (950 MHz ^1H frequency), equipped with a 0.7 mm HCDN MAS probe at 100 kHz MAS. The temperature of the nitrogen cooling gas was set to 252 K with 550 L/h.

In all experiments, the estimated sample temperature (accounting for frictional heating from the MAS) was 288–298 K. For decoupling of the heteronuclear dipolar interactions, SW_f-TPPM[82] was used on the proton channel and WALTZ-16[83] was used on heteronuclear channels. MISSISSIPPI[84] water suppression was applied for proton-detected experiments.

ASSOCIATED CONTENT

Supporting Information

The Supporting Information is available free of charge at https://pubs.acs.org/doi/10.1021/jacsau.3c00312.

Linear drift compensation and SPEPS processing for Topspin 4 (TXT)

Linear drift compensation and SPEPS processing for Topspin 3 (TXT)

Numerical simulations of SPEPS, additional experimental data using SPEPS, TROP, and CP elements for dipolar recoupling, experimental parameters, and Bruker Topspin pulse programs implementing the SPEPS-based sequences (PDF)

AUTHOR INFORMATION

Corresponding Authors

Evgeny Nimerovsky − *Department of NMR based Structural Biology, Max Planck Institute for Multidisciplinary Sciences, Göttingen 37077, Germany;* orcid.org/0000-0003-3002-0718; Email: evni@mpinat.mpg.de

Loren B. Andreas − *Department of NMR based Structural Biology, Max Planck Institute for Multidisciplinary Sciences, Göttingen 37077, Germany;* orcid.org/0000-0003-3216-9065; Email: land@mpinat.mpg.de

Authors

Abel Cherian Varkey − *Department of NMR based Structural Biology, Max Planck Institute for Multidisciplinary Sciences, Göttingen 37077, Germany*

Myeongkyu Kim − *Department of NMR based Structural Biology, Max Planck Institute for Multidisciplinary Sciences, Göttingen 37077, Germany*

Stefan Becker − *Department of NMR based Structural Biology, Max Planck Institute for Multidisciplinary Sciences, Göttingen 37077, Germany*

Complete contact information is available at: https://pubs.acs.org/10.1021/jacsau.3c00312

Author Contributions

CRediT: **Evgeny Nimerovsky** conceptualization, data curation, investigation, methodology, project administration, software, supervision, validation, visualization, writing-original draft, writing-review & editing; **Abel Cherian Varkey** visualization, writing-review & editing; **Myeongkyu Kim** resources, writing-review & editing; **Stefan Becker** resources, writing-review & editing; **Loren B. Andreas** conceptualization, data curation, funding acquisition, methodology, project administration, resources, software, supervision, validation, visualization, writing-original draft, writing-review & editing.

Funding

Open access funded by Max Planck Society.

Notes

The authors declare no competing financial interest.

ACKNOWLEDGMENTS

The authors acknowledge financial support from the MPI for Multidisciplinary Sciences and from the Deutsche Forschungsgemeinschaft (Emmy Noether program Grant AN1316). They thank Melanie Wegstroth and Kerstin Overkamp for excellent help with protein production. They also thank Dr. Dirk Bockelmann and Brigitta Angerstein for technical assistance.

REFERENCES

(1) Andrew, E. R.; Bradbury, A.; Eades, R. G. Nuclear Magnetic Resonance Spectra from a Crystal rotated at High Speed. *Nature* **1958**, *182*, 1659.

(2) Emshwiller, M.; Hahn, E. L.; Kaplan, D. Pulsed Nuclear Resonance Spectroscopy. *Phys. Rev.* **1960**, *118*, 414–424.

(3) Struppe, J.; Quinn, C. M.; Sarkar, S.; Gronenborn, A. M.; Polenova, T. Ultrafast 1H MAS NMR Crystallography for Natural Abundance Pharmaceutical Compounds. *Mol. Pharmaceutics* **2020**, *17*, 674–682.

(4) Nishiyama, Y. Solid-State NMR Under Ultrafast MAS Rate of 40−120 kHz. In *Experimental Approaches of NMR Spectroscopy: Methodology and Application to Life Science and Materials Science*; Springer, 2018; pp 171−195.
(5) Penzel, S.; Oss, A.; Org, M. L.; et al. Spinning faster: protein NMR at MAS frequencies up to 126 kHz. *J. Biomol. NMR* **2019**, *73*, 19−29.
(6) Xue, K.; Sarkar, R.; Motz, C.; et al. Magic-Angle Spinning Frequencies beyond 300 kHz Are Necessary To Yield Maximum Sensitivity in Selectively Methyl Protonated Protein Samples in Solid-State NMR. *J. Phys. Chem. C* **2018**, *122*, 16437−16442.
(7) Nishiyama, Y.; Hou, G.; Agarwal, V.; Su, Y.; Ramamoorthy, A. Ultrafast Magic Angle Spinning Solid-State NMR Spectroscopy: Advances in Methodology and Applications. *Chem. Rev.* **2023**, *123*, 918−988.
(8) Reif, B.; Griffin, R. G. 1H detected 1H,15N correlation spectroscopy in rotating solids. *J. Magn. Reson.* **2003**, *160*, 78−83.
(9) Zhou, D. H.; Shea, J.; Nieuwkoop, A.; et al. Solid-State Protein-Structure Determination with Proton-Detected Triple-Resonance 3D Magic-Angle-Spinning NMR Spectroscopy. *Angew. Chem., Int. Ed.* **2007**, *46*, 8380−8383.
(10) Chevelkov, V.; van Rossum, B. J.; Castellani, F.; et al. H Detection in MAS Solid-State NMR Spectroscopy of Biomacromolecules Employing Pulsed Field Gradients for Residual Solvent Suppression. *J. Am. Chem. Soc.* **2003**, *125*, 7788−7789.
(11) Zhou, D. H.; Shah, G.; Cormos, M.; et al. Proton-Detected Solid-State NMR Spectroscopy of Fully Protonated Proteins at 40 kHz Magic-Angle Spinning. *J. Am. Chem. Soc.* **2007**, *129*, 11791−11801.
(12) Andreas, L. B.; Le Marchand, T.; Jaudzems, K.; Pintacuda, G. High-resolution proton-detected NMR of proteins at very fast MAS. *J. Magn. Reson.* **2015**, *253*, 36−49.
(13) Liang, L.; Ji, Y.; Chen, K.; et al. Solid-State NMR Dipolar and Chemical Shift Anisotropy Recoupling Techniques for Structural and Dynamical Studies in Biological Systems. *Chem. Rev.* **2022**, *122*, 9880−9942.
(14) Ahlawat, S.; Mote, K. R.; Lakomek, N.-A.; Agarwal, V. Solid-State NMR: Methods for Biological Solids. *Chem. Rev.* **2022**, *122*, 9643−9737.
(15) Le Marchand, T.; Schubeis, T.; Bonaccorsi, M.; et al. 1H-Detected Biomolecular NMR under Fast Magic-Angle Spinning. *Chem. Rev.* **2022**, *122*, 9943−10018.
(16) Chien, P.-H.; Griffith, K. J.; Liu, H.; Gan, Z.; Hu, Y.-Y. Recent Advances in Solid-State Nuclear Magnetic Resonance Techniques for Materials Research. *Annu. Rev. Mater. Res.* **2020**, *50*, 493−520.
(17) Barbet-Massin, E.; Pell, A. J.; Retel, J. S.; et al. Rapid Proton-Detected NMR Assignment for Proteins with Fast Magic Angle Spinning. *J. Am. Chem. Soc.* **2014**, *136*, 12489−12497.
(18) Stejskal, E. O.; Schaefer, J.; Waugh, J. S. Magic-angle spinning and polarization transfer in proton-enhanced NMR. *J. Magn. Reson. (1969)* **1977**, *28*, 105−112.
(19) Hartmann, S. R.; Hahn, E. L. Nuclear Double Resonance in the Rotating Frame. *Phys. Rev.* **1962**, *128*, 2042−2053.
(20) Stejskal, E. O.; Schaefer, J.; McKay, R. A. High-resolution, slow-spinning magic-angle carbon-13 NMR. *J. Magn. Reson. (1969)* **1977**, *25*, 569−573.
(21) Dvinskikh, S. V.; Chizhik, V. I. Cross-polarization with radio-frequency field phase and amplitude modulation under magic-angle spinning conditions. *J. Exp. Theor. Phys.* **2006**, *102*, 91−101.
(22) Baldus, M.; Petkova, A. T.; Herzfeld, J.; Griffin, R. G. Cross polarization in the tilted frame: assignment and spectral simplification in heteronuclear spin systems. *Mol. Phys.* **1998**, *95*, 1197−1207.
(23) Kamihara, T.; Takegoshi, K. Rotational resonance for a heteronuclear spin pair under magic-angle spinning in solid-state NMR. *J. Chem. Phys.* **2017**, *146*, No. 154202.
(24) Ladizhansky, V.; Vega, S. Polarization transfer dynamics in Lee−Goldburg cross polarization nuclear magnetic resonance experiments on rotating solids. *J. Chem. Phys.* **2000**, *112*, 7158−7168.
(25) Bjerring, M.; Nielsen, N. C. Solid-state NMR heteronuclear coherence transfer using phase and amplitude modulated rf irradiation at the Hartmann−Hahn sideband conditions. *Chem. Phys. Lett.* **2003**, *382*, 671−678.
(26) Dvinskikh, S. V.; Zimmermann, H.; Maliniak, A.; Sandström, D. Heteronuclear dipolar recoupling in solid-state nuclear magnetic resonance by amplitude-, phase-, and frequency-modulated Lee−Goldburg cross-polarization. *J. Chem. Phys.* **2005**, *122*, No. 044512.
(27) Zhang, Z.; Fu, R.; Li, J.; Yang, J. Asymmetric simultaneous phase-inversion cross-polarization in solid-state MAS NMR: Relaxing selective polarization transfer condition between two dilute spins. *J. Magn. Reson.* **2014**, *242*, 214−219.
(28) Peng, W. K.; Takeda, K.; Kitagawa, M. A new technique for cross polarization in solid-state NMR compatible with high spinning frequencies and high magnetic fields. *Chem. Phys. Lett.* **2006**, *417*, 58−62.
(29) Wi, S.; Schurko, R.; Frydman, L. 1H−2H cross-polarization NMR in fast spinning solids by adiabatic sweeps. *J. Chem. Phys.* **2017**, *146*, No. 104201.
(30) Duan, P.; Schmidt-Rohr, K. Composite-pulse and partially dipolar dephased multiCP for improved quantitative solid-state 13C NMR. *J. Magn. Reson.* **2017**, *285*, 68−78.
(31) Matsunaga, T.; Matsuda, I.; Yamazaki, T.; Ishii, Y. Decoherence optimized tilted-angle cross polarization: A novel concept for sensitivity-enhanced solid-state NMR using ultra-fast magic angle spinning. *J. Magn. Reson.* **2021**, *322*, No. 106857.
(32) Shekar, S. C.; Zhao, W.; Weldeghiorghis, T. K.; Wang, T. Effect of cross polarization radiofrequency phases on signal phase. *Solid State Nucl. Magn. Reson.* **2022**, *117*, No. 101771.
(33) Kolbert, A. C.; Gann, S. L. Variable-effective-field cross polarization. An approach to broadband Hartmann-Hahn matching in MAS NMR. *Chem. Phys. Lett.* **1994**, *224*, 86−90.
(34) Jain, S.; Bjerring, M.; Nielsen, N. C. Efficient and Robust Heteronuclear Cross-Polarization for High-Speed-Spinning Biological Solid-State NMR Spectroscopy. *J. Phys. Chem. Lett.* **2012**, *3*, 703−708.
(35) Basse, K.; Jain, S. K.; Bakharev, O.; Nielsen, N. C. Efficient polarization transfer between spin-1/2 and 14N nuclei in solid-state MAS NMR spectroscopy. *J. Magn. Reson.* **2014**, *244*, 85−89.
(36) Nielsen, A. B.; Tan, K. O.; Shankar, R.; et al. Theoretical description of RESPIRATION-CP. *Chem. Phys. Lett.* **2016**, *645*, 150−156.
(37) Peersen, O. B.; Wu, X. L.; Kustanovich, I.; Smith, S. O. Variable-Amplitude Cross-Polarization MAS NMR. *J. Magn. Reson., Ser. A* **1993**, *104*, 334−339.
(38) Metz, G.; Wu, X. L.; Smith, S. O. Ramped-Amplitude Cross Polarization in Magic-Angle-Spinning NMR. *J. Magn. Reson., Ser. A* **1994**, *110*, 219−227.
(39) Hediger, S.; Meier, B. H.; Ernst, R. R. Adiabatic passage Hartmann-Hahn cross polarization in NMR under magic angle sample spinning. *Chem. Phys. Lett.* **1995**, *240*, 449−456.
(40) Penzel, S.; Smith, A. A.; Agarwal, V.; et al. Protein resonance assignment at MAS frequencies approaching 100 kHz: a quantitative comparison of J-coupling and dipolar-coupling-based transfer methods. *J. Biomol. NMR* **2015**, *63*, 165−186.
(41) Blahut, J.; Brandl, M. J.; Pradhan, T.; Reif, B.; Tošner, Z. Sensitivity-Enhanced Multidimensional Solid-State NMR Spectroscopy by Optimal-Control-Based Transverse Mixing Sequences. *J. Am. Chem. Soc.* **2022**, *144*, No. 17336.
(42) Cavanagh, J.; Rance, M. Sensitivity improvement in isotropic mixing (TOCSY) experiments. *J. Magn. Reson. (1969)* **1990**, *88*, 72−85.
(43) States, D. J.; Haberkorn, R. A.; Ruben, D. J. A two-dimensional nuclear overhauser experiment with pure absorption phase in four quadrants. *J. Magn. Reson. (1969)* **1982**, *48*, 286−292.
(44) Palmer, A. G.; Cavanagh, J.; Wright, P. E.; Rance, M. Sensitivity improvement in proton-detected two-dimensional heteronuclear correlation NMR spectroscopy. *J. Magn. Reson. (1969)* **1991**, *93*, 151−170.
(45) Schleucher, J.; Sattler, M.; Griesinger, C. Coherence Selection by Gradients without Signal Attenuation: Application to the Three-

https://doi.org/10.1021/jacsau.3c00312
JACS Au 2023, 3, 2763−2771

Dimensional HNCO Experiment. *Angew. Chem., Int. Ed.* **1993**, *32*, 1489−1491.
(46) Slichter, C. P. *Principles of Magnetic Resonance*; Springer Berlin Heidelberg, 1990.
(47) Kiihne, S.; Mehta, M. A.; Stringer, J. A.; et al. Distance Measurements by Dipolar Recoupling Two-Dimensional Solid-State NMR. *J. Phys. Chem. A* **1998**, *102*, 2274−2282.
(48) Tycko, R. Sensitivity Enhancement in Two-Dimensional Solid-State NMR Spectroscopy by Transverse Mixing. *ChemPhysChem* **2004**, *5*, 863−868.
(49) Herbst, C.; et al. 13C−13C Chemical Shift Correlation in Rotating Solids without 1H Decoupling During Mixing. *ChemPhysChem* **2007**, *8*, 1770−1773.
(50) Khaneja, N. Sensitivity enhanced recoupling experiments in solid-state NMR by γ preparation. *J. Magn. Reson.* **2006**, *183*, 242−251.
(51) Lin, J.; Griffin, R. G.; Nielsen, N. Chr.; Khaneja, N. Three pulse recoupling and phase jump matching. *J. Magn. Reson.* **2016**, *263*, 172−183.
(52) Lin, J.; Griffin, R. G.; Khaneja, N. Recoupling in solid state NMR using γ prepared states and phase matching. *J. Magn. Reson.* **2011**, *212*, 402−411.
(53) Gopinath, T.; Veglia, G. Sensitivity Enhancement in Static Solid-State NMR Experiments via Single- and Multiple-Quantum Dipolar Coherences. *J. Am. Chem. Soc.* **2009**, *131*, 5754−5756.
(54) Gopinath, T.; Traaseth, N. J.; Mote, K.; Veglia, G. Sensitivity Enhanced Heteronuclear Correlation Spectroscopy in Multidimensional Solid-State NMR of Oriented Systems via Chemical Shift Coherences. *J. Am. Chem. Soc.* **2010**, *132*, 5357−5363.
(55) Gopinath, T.; Mote, K. R.; Veglia, G. Sensitivity and resolution enhancement of oriented solid-state NMR: Application to membrane proteins. *Prog. Nucl. Magn. Reson. Spectrosc.* **2013**, *75*, 50−68.
(56) Hansen, S. K.; Bertelsen, K.; Paaske, B.; Nielsen, N. Chr.; Vosegaard, T. Solid-state NMR methods for oriented membrane proteins. *Prog. Nucl. Magn. Reson. Spectrosc.* **2015**, *88*−*89*, 48−85.
(57) Gullion, T.; Baker, D. B.; Conradi, M. S. New, compensated Carr-Purcell sequences. *J. Magn. Reson. (1969)* **1990**, *89*, 479−484.
(58) Nimerovsky, E.; Becker, S.; Andreas, L. B. Windowed cross polarization at 55 kHz magic-angle spinning. *J. Magn. Reson.* **2023**, *349*, No. 107404.
(59) Laage, S.; Marchetti, A.; Sein, J.; et al. Band-Selective 1H−13C Cross-Polarization in Fast Magic Angle Spinning Solid-State NMR Spectroscopy. *J. Am. Chem. Soc.* **2008**, *130*, 17216−17217.
(60) Wu, X. L.; Zilm, K. W. Cross Polarization with High-Speed Magic-Angle Spinning. *J. Magn. Reson., Ser. A* **1993**, *104*, 154−165.
(61) Tošner, Z.; Purea, A.; Struppe, J. O.; et al. Radiofrequency fields in MAS solid state NMR probes. *J. Magn. Reson.* **2017**, *284*, 20−32.
(62) Tošner, Z.; Sarkar, R.; Becker-Baldus, J.; et al. Overcoming Volume Selectivity of Dipolar Recoupling in Biological Solid-State NMR Spectroscopy. *Angew. Chem., Int. Ed.* **2018**, *57*, 14514−14518.
(63) Taware, P. P.; Jain, M. G.; Raran-Kurussi, S.; et al. Measuring Dipolar Order Parameters in Nondeuterated Proteins Using Solid-State NMR at the Magic-Angle-Spinning Frequency of 100 kHz. *J. Phys. Chem. Lett.* **2023**, *14*, 3627−3635.
(64) Šmelko, A.; Blahut, J.; Reif, B.; Tošner, Z. Performance of the cross-polarization experiment in conditions of radiofrequency field inhomogeneity and slow to ultrafast magic angle spinning (MAS). *Magn. Reson.* **2023**, *4*, 199−215.
(65) Campbell, G. C.; Galya, L. G.; Beeler, A. J.; English, A. D. Effect of RF Inhomogeneity upon Quantitative Solid-State NMR Measurements. *J. Magn. Reson., Ser. A* **1995**, *112*, 225−228.
(66) Paulson, E. K.; Martin, R. W.; Zilm, K. W. Cross polarization, radio frequency field homogeneity, and circuit balancing in high field solid state NMR probes. *J. Magn. Reson.* **2004**, *171*, 314−323.
(67) Gupta, R.; Hou, G.; Polenova, T.; Vega, A. J. RF Inhomogeneity and how it Control CPMAS. *Solid State Nucl. Magn. Reson.* **2015**, *72*, 17−26.
(68) Berns, A. E. Effect of RF Field Inhomogeneity and Sample Restriction on Spectral Resolution of CP/MAS-13C NMR Spectra of Natural Organic Matter. *Open Magn. Reson. J.* **2010**, *3*, 75−83, DOI: 10.2174/1874769801003010075.
(69) Blahut, J.; Brandl, M. J.; Sarkar, R.; Reif, B.; Tošner, Z. Optimal control derived sensitivity-enhanced CA-CO mixing sequences for MAS solid-state NMR − Applications in sequential protein backbone assignments. *J. Magn. Reson. Open* **2023**, *16*−*17*, No. 100122.
(70) Wong, L. E.; Maier, J.; Wienands, J.; Becker, S.; Griesinger, C. Sensitivity-Enhanced Four-Dimensional Amide−Amide Correlation NMR Experiments for Sequential Assignment of Proline-Rich Disordered Proteins. *J. Am. Chem. Soc.* **2018**, *140*, 3518−3522.
(71) Najbauer, E. E.; Andreas, L. B. Correcting for magnetic field drift in magic-angle spinning NMR datasets. *J. Magn. Reson.* **2019**, *305*, 1−4.
(72) Andreas, L. B.; Reese, M.; Eddy, M. T.; et al. Structure and Mechanism of the Influenza A M218−60 Dimer of Dimers. *J. Am. Chem. Soc.* **2015**, *137*, 14877−14886.
(73) Baldus, M.; Geurts, D. G.; Hediger, S.; Meier, B. H. Efficient15N−13C Polarization Transfer by Adiabatic-Passage Hartmann−Hahn Cross Polarization. *J. Magn. Reson., Ser. A* **1996**, *118*, 140−144.
(74) Ernst, M.; Meier, B. H. Adiabatic Polarization-Transfer Methods in MAS Spectroscopy. In *Encyclopedia of Magnetic Resonance*; John Wiley & Sons, Ltd., 2010.
(75) Li, Y.; Berthold, D. A.; Frericks, H. L.; Gennis, R. B.; Rienstra, C. M. Partial 13C and 15N Chemical-Shift Assignments of the Disulfide-Bond-Forming Enzyme DsbB by 3D Magic-Angle Spinning NMR Spectroscopy. *ChemBioChem* **2007**, *8*, 434−442.
(76) Schuetz, A.; Wasmer, C.; Habenstein, B.; et al. Protocols for the Sequential Solid-State NMR Spectroscopic Assignment of a Uniformly Labeled 25 kDa Protein: HET-s(1−227). *ChemBioChem* **2010**, *11*, 1543−1551.
(77) Nimerovsky, E.; Goldbourt, A. Insights into the spin dynamics of a large anisotropy spin subjected to long-pulse irradiation under a modified REDOR experiment. *J. Magn. Reson.* **2012**, *225*, 130−141.
(78) Schnell, J. R.; Chou, J. J. Structure and mechanism of the M2 proton channel of influenza A virus. *Nature* **2008**, *451*, 591−595.
(79) Andreas, L. B.; Eddy, M. T.; Pielak, R. M.; Chou, J.; Griffin, R. G. Magic Angle Spinning NMR Investigation of Influenza A M218−60: Support for an Allosteric Mechanism of Inhibition. *J. Am. Chem. Soc.* **2010**, *132*, 10958−10960.
(80) Hoyer, W.; Antony, T.; Cherny, D.; et al. Dependence of α-Synuclein Aggregate Morphology on Solution Conditions. *J. Mol. Biol.* **2002**, *322*, 383−393.
(81) Maurer, A.; Leonov, A.; Ryazanov, S.; et al. 11C Radiolabeling of anle253b: a Putative PET Tracer for Parkinson's Disease That Binds to α-Synuclein Fibrils in vitro and Crosses the Blood-Brain Barrier. *ChemMedChem* **2020**, *15*, 411−415.
(82) Thakur, R. S.; Kurur, N. D.; Madhu, P. K. Swept-frequency two-pulse phase modulation for heteronuclear dipolar decoupling in solid-state NMR. *Chem. Phys. Lett.* **2006**, *426*, 459−463.
(83) Shaka, A. J.; Keeler, J.; Frenkiel, T.; Freeman, R. An improved sequence for broadband decoupling: WALTZ-16. *J. Magn. Reson. (1969)* **1983**, *52*, 335−338.
(84) Zhou, D. H.; Rienstra, C. M. High-performance solvent suppression for proton detected solid-state NMR. *J. Magn. Reson.* **2008**, *192*, 167−172.

https://doi.org/10.1021/jacsau.3c00312
JACS Au 2023, 3, 2763−2771